"Study of Combustion Mechanism of Nitramine-Polymer Mixtures"

Final Technical Report
by
Anatoli A.Zenin

August, 2000

United States Army

EUROPEAN RESEARCH OFFICE OF THE U.S.ARMY

London, England

CONTRACT NUMBER N68171-99-M-6238
Reference number R&D ~~8732-CH07~~ 8724-AN-01

Russian Academy of Sciences,
Semenov Institute of Chemical Physics
Russia

Approved for Public Release; distribution unlimited

REPORT DOCUMENTATION PAGE			Form Approved OMB No. 0704-0188
1. AGENCY USE ONLY	2. REPORT DATE 30 August 2000	3. REPORT TYPE AND DATES COVERED Final Report; 30 June 1999 - 30 August 2000	
4. TITLE AND SUBTITLE "Study of Combustion Mechanism of Nitramine-Polymer Mixtures"			5. FUNDING NUMBERS C
6. AUTHOR Anatoli A. Zenin			
7. PERFORMING ORGANISATION NAME AND ADDRESS Senenov Institute of Chemical Physics, Russian Academy of Sciences Kosygin Street 4, 117977 Moscow, Russia			8.PERFORMING ORGANISATION REPORT NUMBER -
9. SPONSORING/MONITORING AGENCY NAME AND ADDRESS Mr. Jon Flower U.S. Naval Regional Contracting Center, Detachment London, Department of Environment Complex, Block 2, Wing 12. Eastcote Road, Ruislip, Middlesex HA4 8BS			10. SPONSORING/MONITORING AGENCY REPORT NUMBER
11. SUPPLEMENTARY NOTES			
12a. DISTRIBUTION/AVAILABILITY STATEMENT			12b. DISTRIBUTION CODE

13. ABSTRACT

Combustion mechanisms of mixtures with energetic binders and nitramines (RDX, HMX) were studied in wide region of pressures and initial temperatures. 8 mixtures having 4 modern energetic binders were investigated. Temperature profiles of burning waves were obtained by microthermocouple techniques. 17 characteristics of the waves were established for every mixture and every combustion regime by measurements and data processing. Temperature and pressure sensitivities of burning rate and surface temperature were estimated. Criteria of stable combustion were determined. Characteristic features of the combustion mechanisms were described. It was established, partly, that significant heat release in solid and weak heat feedback from gas to solid are observed for all mixtures. The control region which governs the burning rate is located in solid part of the combustion waves and in a thin gas layer close to the burning surface. Burning rate responce functions to oscillatory pressure were found. Comparisons of combustion mechanisms of mixtures with energetic binders and mixtures with HTPB were made. Obtained data provide base for modelling different combustion phenomena of these mixtures.

14. SUBJECT ITEMS	15. NUMBER OF PAGES
energetic binders/nitramines, combustion mechanisms, thermophysical parameters of combustion waves, macrokinetics of gasification, burning rate control regions, temperature and pressure sensitivities, data for modelling, burning rate responce functions to oscillatory pressure.	26
	16. PRICE CODE NTIS

17. SECURITY CLASSIFICATION OF REPORT	18. SECURITY CLASSIFICATION OF THIS PAGE	19 SECURITY CLASSIFICATION OF ABSTRACT	20. LIMITATION OF ABSTRACT
UNCLASSIFIED	UNCLASSIFIED	UNCLASSIFIED	UL

Body of the Report

1. Background of the Problem

It is well known that mixtures of cyclic nitramine-polymer binder offer many advantages for advanced propulsions. They have better performances (large amount of gas, high specific impulse for rockets and impetus for guns), safety (low sensitivity) and environment friendness (nontoxic and noncorrosive combustion products). Energetic binders are preferable for that propulsions. The study of combustion mechanism of the nitramine-energetic polymer binder mixtures is very important. The understanding of the mechanisms is useful for many applications of that propulsions.

Different mixtures based on new energetic binders were studied in this work. Especially detailed were studied mixtures with improved characteristics.

2. Approach

Different types of energetic binders were used during the contract period. They were: glycidyl azide polymer with molecular mass of two thousand (GAP2), copolymer of two thermoplastic elastomers - poly bis 3,3-azidomethyloxetane (BAMO) and poly 3-azidomethyl-3-methyloxetane (AMMO), in proportion 50:50, copolymer of BAMO with tetrahydrofuran (THF), in proportion 50:50, and glycidyl azide-polyurethane copolymer (GAP1U). Cyclic nitramines HMX and RDX are used as oxidizers. The ratio 20:80 for components of energetic binder/nitramine was used for all of the mixtures. Nitramine powders have the following characteristics: 50% by weight have sizes <50 microns and 50% - 150-300 microns. Purity of HMX and RDX was 99%. The propellant samples were 0.8cm in diameter and 2 cm in length.

Thus the following mixtures were prepared and investigated: 1) GAP2/HMX, 2) GAP2/RDX, 3) (BAMO-AMMO)/HMX, 4) (BAMO-AMMO)/RDX, 5) (BAMO-THF)/HMX, 6) (BAMO-THF)/RDX and 7) GAP1U/HMX, 8) GAP1U/RDX.

The study of the combustion mechanism of the mixtures was performed by obtaining geometrical and thermal structure of burning waves of the mixtures and by processing of the obtained data. The peculiarity of the work is the measurement of all characteristics of combustion waves under change of external parameters - pressure and initial sample temperature. This approach allows one to established distinctive features of the combustion mechanism of the studied mixtures.

The most reliable data were received for mixtures 1) GAP2/HMX, 2) GAP2/RDX and 3) (BAMO-AMMO)/HMX, 4) (BAMO-AMMO)/RDX. Because of that temperature and pressure sensitivities of burning rate and surface temperature were obtained for these mixtures. Burning rate response functions to oscillatory pressure were estimated by using these sensitivities.

3. Experimental Techniques.

3.1. Conditions of experiments and microthermocouple techniques.

Temperature profiles of the combustion waves and the burning surface temperatures were obtained by microthermocouple methods. Profiles of the combustion waves were obtained by microthermocouples imbedded into solid. Thermocouples went through combustion waves when the waves propagated through the solid samples and registered temperature profiles. The ribbon U-shaped thermocouples made of alloys W+5%Re/W+20%Re of 2-7mkm thick were imbedded into the samples. Cylindrical samples of 8 mm in diameter and 3 cm in length were cat by small thin knife of U-shape form, thermocouple placed into the created cross-sections, which were moistend by acetone, and the joined sections with thermocouples inside were protected by thin layer of polymer glue. Sample drying was performed during 6 ours. Every sample had inside 2-3 thermocouples placed one above the other. Distances between the junctions were 2-4 mm. The samples were burned in a bomb of constant pressure in atmosphere of nitrogen at pressures 5-100atm and at sample initial temperatures T_o= -100, +20, and +90°C. In experiments at elevated sample temperatures the sample was placed into a small thermostat inside the bomb. The sample heating was controlled by thermocouples. Samples were ignited by electrically heated wire. Thermocouple signals were registered by amplifier and oscillograph. Burning rate was measured by time delay between the thermocouple signals, by photoregistrations of sample combustion and by pressure increase during the sample combustion. Photoregistration of sample combustion allows also the type of combustion to be established. Burning

surface temperatures were measured by thermocouples that are being pressed to the surface during sample combustion and by establishing the locations of slope breaks on temperature profiles registered by thermocouples (see below).

3.2. Temperature profile measurement validations. As a rule, temperature gradient close to the burning surface has a very high value. It implies that thermocouple measurements can give temperature profiles with significant errors due to thermocouple heat inertia. Because of that it is necessary to find conditions under which thermocouple measurements in combustion waves will introduce small errors. These conditions have been found by numerical simulations. The thermocouple partially absorbs the heat of the thermal layer and decreases the temperature at the point of the measurement. The requirement of small temperature error (less than 10%) of the thermocouple is indicated by the following formula: $h<0.2\ \chi/r_b$;

Here: h - thermocouple thickness (in cm), χ- heat diffusivity of the solid (in cm^2/s), r_b - linear burning rate (in cm/s). $\chi/r_b=l$ where l is the thickness of heat layer of the condensed phase. There is another requirement for correct measurements: the thermocouples have to have U-shape form. It is necessary because of a very high difference between heat conduction coefficients of metallic thermocouple wire and that of solid or gas. Junctions of U-shaped thermocouples do not experience large temperature decrease. Modelling experiments and numerical simulations show that the decrease of junction temperature will be small (≤3%) if the horizontal part of the U-shaped thermocouple is about one hundred times more than thermocouple thickness h. Thermal inertia of the thermocouple in the gas phase can be taken into consideration and eliminated by a correction procedure. The procedure implies the use of the following equation:

$$dT_{ex}/dx=(r_b\tau_o)^{-1}\cdot(T - T_{ex});$$

Here: T - the real temperature of gas in the combustion wave; T_{ex} - the temperature registrated by thermocouple; τ_o - time response of the thermocouple in gas. Time response depends on mass burning rate m ($m=\rho\cdot r_b$) and temperature T. The temperature profiles in gas were corrected by this equation. The theory of thermocouple measurements in combustion waves of solids was created and confirmed by measurements of combustion wave temperature profiles by thermocouples with sequentially decreased thickness (method of "zero diameter"). All the above mentioned requirements have been met in the investigations. Different types of metal wires for thermocouples were used (We,Re and Pt,Rh) to test the catalytic effect on thermocouples. The catalytic effect was not observed. The method of burning surface temperature measurement by determining locations of slope breaks on temperature profiles registered by thermocouples (method of "slope break") is based on the existence of the delay ($r_b\ \tau_o$) on the temperature profiles when thermocouples go through the burning surface. The delay is due to the change of heat exchange between environment and thermocouple: contact heat exchange in solid is replaced by convective heat exchange in gas.

4. Results of Measurements and Processing for Mixtures 1-4

As it was mentioned above, four new mixtures - 1 - 4 -, were detailed studied. The mixtures had more uniform contents which allow decreased scattering of all characteristics to be obtained. The samples had increased solid density ρ and improved mechanical properties. The thermodynamic calculated adiabatic flame temperatures T_{ad} are equal to 2595-2787 K.

The characteristics of the initial mixtures were as follows:

1) GAP2/HMX, ρ=1,52 g/cm^3; sum formula: $O_{24.156}H_{21.811}N_{26.886}C_{17.896}$; T_{ad}=2776 K;

2) GAP2/RDX, ρ=1,51 g/cm^3; sum formula: $O_{24.156}H_{21.811}N_{26.886}C_{17.896}$; T_{ad}=2787 K;

3) [BAMO-AMMO]/HMX, ρ=1, 63g/cm^3; sum formula: $O_{23.88}H_{32.24}N_{26.37}C_{18.06}$; T_{ad}=2595 K;

4) [BAMO-AMMO]/RDX, ρ=1,56 g/cm^3; sum formula: $O_{23.88}H_{32.24}N_{26.31}C_{18.06}$; T_{ad}=2606 K;

Carbon residue on the burning surface of the mixtures did not observed.

4.1. Temperature Profiles and Burning Wave Characteristics.

Temperature profiles for the mixtures were obtained at pressures 5-100 atm since at p<5 atm the mixtures can not burn stable and their ignition is very difficult. The obtained temperature profiles have stable character, show a small date scattering, and, as a rule, have not regular pulsations (only at 5 atm some of samples have irregular temperature pulsations of ~ 200° in amplitude). 10-12 temperature curves were received for every regime of combustion and then averaging of these curves was performed. Thus every regime of combustion presented below is outlined by one

averaged temperature profile. Figures 1, 2 show the obtained averaged temperature profiles of mixtures 1, 2 (GAP2/HMX and GAP2/RDX) and mixtures 3, 4 [(BAMO-AMMO)/HMX and (BAMO-AMMO)/RDX] at pressure 5 atm and sample initial temperature T_o=20°C. Figures 3-6 show the obtained averaged temperature profiles of mixture 1 at pressures p=10, 20 50 and 100 atm and at T_o=-100, 20 and +90°C. Figures 7-10 show the averaged profiles for mixture 2, Figs. 11-14 - for mixture 3, and Figs. 15-18 - for mixture 4, under the same conditions. The presented Figs. show that the gas phase of the combustion waves of the investigated mixtures is comprised of one or two zones. The first zone of the two-zone structure is a relatively low-temperature zone with a zone temperature T_1, and the second zone is the flame zone with the final temperature T_f. At elevated pressures (at p>20 atm) the two zones always merged into one zone. Adiabatic flame temperature T_{ad} is achieved at about 50-80 atm under the investigated conditions.

Tables 1, 2, 3 and 4 show the averaged burning wave parameters obtained by experiments and by processing experimental data for every mixture (see below). Small corrections of the experimental data were performed during preparations of the Final Report.

4.1.1. *Mass burning rates.* Tables 1-4 show that mass burning rates m of all mixtures increase when pressure p and sample initial temperature T_o increase. Values of m for mixtures 1-4 are close each other, but the mixtures with RDX have a bit more values of m. Mass burning rates of the investigated mixtures increase from 0.10-0.12 g/cm^{2}s at 5 atm up to 1.2 1.5 g/cm^{2}s at 100 atm. Values of m of the investigated mixtures at 10 atm increase from 0.21-0.22 g/cm^{2}s at T_o=20°C up to 0.2-0.28 g/cm^{2}s at T_o=+90°C and decrease to 0.15-0.16 g/cm^{2}s at T_o=-100°C. Difference between values of m at different T_o increases with pressure. For instance, at 80 atm m=0.94-1.1 g/cm^{2}s at T_o=-100°C, and m=1.25-1.42 g/cm^{2}s at T_o=+90°C. Standard deviation of mass burning rate measurements is ϑm=±5%.

4.1.2. *Burning surface temperatures.* Tables 1-4 show that burning surface temperature T_s always increases when T_o and pressure increase. Values of T_s for mixtures 1-4 are also close each other and increase from 330-335°C at 5 atm up to 492-500°C (T_o=20°C) at 100 atm. Difference between values of T_s at different T_o decreases when pressure increases. For instance, at 10 atm T_s is equal to 345-350°C at T_o=-100°C and to 375-380°C at T_o=+90°C, but at 80 atm T_s comprises 475-480°C at T_o=-100°C and 490-500°C at T_o=+90°C Standard deviation of burning surface temperature measurements is ϑT_s=±5%.

4.1.3. *Geometric structures of temperature profiles in gas.* As it was mentioned above, the gas phase of the burning waves of the studied mixtures has two type of the structure: single-zone and two-zone structures. The mixtures always have two-zone structure at p<10-20 atm and both zones merge at 20-50 atm. Values of mean temperature of the first flame T_1 are equal to 900-980°C at 5 atm and increase up to 1000-1100°C at 20 atm. Influence of T_o on T_1 is very week. Please, note that mark - in Tables 1-4 implies that the parameter, T_1 in this case, does not exist in this regime.

Flame temperatures T_f are small at 5 atm (1800-1950°C) and increase when pressure increases up to thermodynamically calculated values of the temperatures at 50-80 atm. As a rule, values of T_f increase approximately on the value of (T_o-20°) when sample temperature changes.

Distances L_1 between the burning surface and the beginning of the flame zone decrease when preesure increases. In fact, L_1 is the length of the first flame. Values of L_1 are equal to 300-800 μm at 5 atm and decrease up to 100-200 μm at 20 atm. Sample initial temperature T_o significantly influences on values of L_1: increasing of T_o prolongs L_1 and can creates two-sone structure in the case in which at smaller T_o was one-zone structure. For instance, mixtures 1 and 2 at T_o=20°C have not two zones at p>10 atm, but at T_o=+90°C two-zone structure came to existence at 20 atm.

Tables and Figs. also show that at 10 atm values of L_1 of all mixtures increase 1.5-2 times when T_o increases from 20° up to +90°C.

Distances L between the burning surface and the flame (up to 0.99 T_f) also decrease when preesure increases. In fact, L is the length of the gas phase reaction zone. Values of L are equal to 2-2.5 mm at 5atm and decrease up to 1.0-1.5 mm at 100 atm. As a rule, increasing T_o increases L and decreasing T_o decreases L. The decreasing can be very significant: for instance, values L of mixture 4 decrease about 2 times at 10 atm when T_o decreases from 20 up to -100°C.
Standard deviations of thickness L_1 measurements are ±(20-40)% and that of L are ±(10-20)%.

Table 1: Burning wave parameters of mixture 1 (GAP2/HMX)

No	p, atm	5	10	20	50	80	100
	T_o, °C	20	-100/20/90	-100/20/90	-100/20/90	-100/20/90	-100/20
1	m, g/cm²s	0.1	0.155/0.21/ 0.26	0.28/0.37/ 0.43	0.64/0.77/ 0.88	0.94/1.08/ 1.25	1.1/1.26
2	T_s, °C	330	345/365/375	380/400/410	445/460/470	475/483/490	485/492
3	$\varphi \cdot 10^{-4}$, K/cm	3.5	2.0/4.0/5.0	3.5/5.0/7.8	9.0/10/11	11/11.7/12.4	11.5/12
4	q, cal/g	64	35/37/42	29/31/43	35/30/33	29/28/26	27/25
5	q_r, cal/g	14	13/8/9	8/7/8	5/5/5	4/3.7/3.4	3.4/3.2
6	Q, cal/g	65	140/112/82	174/133/96	212/160/134	216/173/150	223/180
7	l, μm	167	150/107/106	108/77/74	50/58/53	53/49/49	48/48
8	l_m, μm	45	30/40/55	30/35/40	40/30/38	20/30/35	20/20
9	$\chi \cdot 10^3$, cm²/s	1.2	1.2/1.5/1.8	2/2/2.2	2.7/2.9/3.2	3.2/3.5/3.8	3.5/3.8
10	$\lambda_s \cdot 10^4$, cal/cm·s·K	7.3	7.3/9.1/10.8	12/12/13	16.4/18/19.4	19.4/21.2/23	21.2/23
11	T_1, °C	980	-/1050/1000	-/-/1100	-/-/-	-/-/-	-/-
12	T_f, °C	1900	1950/2050/ 2150	2150/2200/ 2280	2400/2500/ 2550	2400/2500 2550	2400/ 2550
13	L_1, μm	600	-/500/900	-/-/350	-/-/-	-/-/-	-/-
14	L, mm	2.0	1.5/2.3/2.3	1.5/1.6/2.3	2.0/2.0/2.5	1.7/1.5/2	1.5/1.7
15	9, μm	43	43/24/19	20/15/13	21/8.0/7.0	6.5/5.7/4.9	5.6/4.9
16	$\lambda_g \cdot 10^4$, cal/cm·s·K	2.0	2.1/2.2/2.2	2.3/2.3/2.4	2.5/2.6/2.6	2.6/2.6/2.6	2.6/2.6
17	Φ_o, kcal/cm³s	1.4	1.3/3.5/5.5	4.1/7.8/14	24/32.7/41	44/53.7/66	53.8/64

Please, note: mark - in the Table implies that the parameter does not exist in this regime.

4.1.4. *Characteristic sizes in gas and solid.*
Characteristic thickness l and l_m in solid presented on Tables 1-4 were obtained by temperature distributions in solid. Experimentally obtained thickness of heat layer in solid l is a distance between the burning surface and a section in solid with temperature $T^*=(T_s-T_o)/e - T_o$ (e is the base of ln). Thickness of partly melt layer (with melt nitramine) in solid l_m is a distance between the burning surface and a section in solid with RDX or HMX melt temperatures T_m which are equal to 200°C for RDX and 280°C for HMX. Values of l and l_m decrease, as a rule, when pressure increases, and $l>l_m$. Conductive sizes 9 of the gas phase were obtained by formula: $9=\lambda_g/mc_p$; where λ_g is

coefficient of heat conduction in gas and c_p is coefficient of specific heat of the gas phase. Values λ_g and c_p were estimated by content of combustion products. The obtained dependencies of $\lambda_g(T_s)$ and $c_p(T_s)$ are presented on Tables 1-4. The Tables show that values ϑ decrease when pressure increases and they are equal to 40-51 μm at 5 atm and to 4-5 μm at 100 atm. It is obvious that $\vartheta << L_1$ and $\vartheta << L$.

Table 2: Burning wave parameters of mixture 2 (GAP2/RDX)

No	p, atm	5	10	20	50	80	100
	T_o, °C	20	-100/20/90	-100/20/90	-100/20/90	-100/20/90	-100/20
1	m, g/cm²s	0.11	0.15/0.21/ 0.27	0.3/0.4/ 0.47	0.65/0.84/ 0.96	0.98/1.25/ 1.42	1.2/1.51
2	T_s, °C	330	345/365/380	385/405/420	450/468/478	480/492/500	490/500
3	$\varphi \cdot 10^{-4}$, K/cm	2.0	3.0/3.5/4.5	4.5/5.0/7.0	8.5/9.5/12	11.2/12.5/ 14.7	12.8/14
4	q, cal/g	38	47/37/37	35/29/36	31/28/31	29/26/27	28/24
5	q_r, cal/g	15	13/10/9	7/6.3/6.3	5.3/4.6/4.8	3.8/3.2/3	3.3/3
6	Q, cal/g	95	141/113/93	176/142/113	207/170/142	223/183/157	228/190
7	l, μm	165	120/106/100	100/85/72	63/54/50	52/48/45	48/40
8	l_m, μm	110	55/75/100	55/65/70	45/50/68	40/40/40	40/38
9	$\chi \cdot 10^3$, cm²/s	1.2	1.2/1.5/1.8	1.8/2/2.2	2.7/3.0/3.2	3.3/3.8/4.0	3.8/4.2
10	$\lambda_s \cdot 10^4$, cal/cm·s·K	7.2	7.3/9.0/10.3	11/12/13	16/18/19	20/23/24	23/25
11	T_1, °C	950	850/950/ 1050	-/-/1100	-/-/-	-/-/-	-/-
12	T_f, °C	1950	2050/2100/ 2180	2100/2200/ 2300	2400/2500/ 2580	2420/2515 2580	2420/ 2515
13	L_1, μm	700	400/500/600	-/-/200	-/-/-	-/-/-	-/-
14	L, mm	2.2	1.5/1.8/2.2	1.7/2.0/2.0	1.5/2.0/2.5	1.5/1.6/1.5	1.2/1.2
15	ϑ, μm	46	34/25/19	17.5/14/12	9.0/7.0/6.0	6.0/5.0/4.0	5.0/4.0
16	$\lambda_g \cdot 10^4$, cal/cm·s·K	2.1	2.2/2.2/2.2	2.2/2.3/2.4	2.4/2.5/2.5	2.5/2.5/2.6	2.5/2.6
17	Φ_o, kcal/cm³s	0.9	2.0/3.1/5.1	5.7/8.4/13.8	23.2/34/49	47/66/89	65/90

4.1.5. *Coefficients of heat diffusivity and heat conductivity in solid heat layer.*

The coefficients of solid heat diffusivity were obtained by formula $\chi = l \cdot r_b$. Tables 1-4 show that χ increases when pressure increases - from $1.2 \cdot 10^{-3}$ cm²/s at 5 atm up to $4 \cdot 10^{-3}$ cm²/s at 100 atm. That are normal values of χ for solid heat layer of many propellant mixtures. Values of χ increase when T_o increases. The coefficients of solid heat conduction were obtained by formula $\lambda_s = \chi \cdot c \cdot \rho$. It was assumed that solid specific heat c=0.4 cal/g·K. Tables show that λ_s increases with pressure - from $(7.2\text{-}7.8) \cdot 10^{-4}$ cal/cm·s·K at 5 atm up to $(24\text{-}26) \cdot 10^{-4}$ cal/cm·s·K at 100 atm. Values of λ_s slightly increase with T_o.

Table 3: Burning wave parameters of mixture 3 ([BAMO-AMMO]/HMX)

No	p, atm	5	10	20	50	80	100
	T_o, °C	20	-100/20/90	-100/20/90	-100/20/90	-100/20/90	-100/20
1	m, g/cm²s	0.1	0.16/0.22/ 0.28	0.32/0.41/ 0.48	0.72/0.85/ 0.98	1.06/1.21/ 1.37	1.24/ 1.44
2	T_s, °C	330	345/365/380	390/407/420	460/470/480	483/490/495	492/500
3	$\varphi \cdot 10^{-4}$, K/cm	2.2	3.4/3.7/5.0	5.0/6.0/6.5	8.0/9.0/11	9.6/11/13.3	10.4/12
4	q, cal/g	46	44.6/37/41	36/34/33	27/26/29	23/24/25	22/22
5	q_r, cal/g	13.8	10/8.2/7.7	7.3/5.7/6.2	3.8/3.5/3.3	2.6/2.5/2.3	2.4/2.0
6	Q, cal/g	83	142/112/86	172/136/113	213/170/143	227/181/154	232/187
7	l, μm	194	143/111/100	100/80/77	46/58/55	54/50/48	53/45
8	l_m, μm	35	35/35/40	30/35/40	25/30/45	20/30/35	20/30
9	$\chi \cdot 10^3$, cm²/s	1.2	1.3/1.5/1.7	1.8/2.0/2.2	2.8/3.0/3.3	3.5/3.7/4.8	3.8/4.0
10	$\lambda_s \cdot 10^4$, cal/cm·s·K	7.8	8.5/9.8/11.0	11.7/13/14	18/19.5/21.5	22.8/24/26	24.7/26
11	T_1, °C	900	-/1020/1050	-/-/-	-/-/-	-/-/-	-/-
12	T_f, °C	1850	1950/2000/ 2100	2150/2200/ 2300	2220/2300/ 2350	2220/2320 2350	2220/ 2320
13	L_1, μm	500	-/400/700	-/-/-	-/-/-	-/-/-	-/-
14	L, mm,	2.2	1.7/1.7/2.0	1.7/2.0/2.0	1.2/1.8/2.0	1.1/1.3/1.5	1.0/0.9
15	ϑ, μm	51	32/24/20	17/13/12	8.3/7.0/6.2	5.8/5.0/4.5	4.9/4.0
16	$\lambda_g \cdot 10^4$, cal/cm·s·K	2.1	2.1/2.2/2.3	2.3/2.3/2.4	2.5/2.5/2.6	2.6/2.6/2.6	2.6/2.6
17	Φ_o, kcal/cm³s	0.9	2.2/3.4/5.9	6.7/10.3/13.0	24/32.5/45.8	43/56.6/77.4	54.8/73

4.1.6. *Heat release in solid and heat feedback from gas into solid.*

The temperature profiles and burning surface temperatures allow the important heat parameters of the burning waves to be estimated. Heat flux from gas to solid $q \cdot m$ by heat conduction is as follows:

$$q \cdot m = -\lambda_g(T) \cdot (dT/dx)_o;$$

Here: $(dT/dx)_o = \varphi$ is the temperature gradient in gas close to the burning surface. Heat feedback from gas into solid by heat conduction q is as follows:

$$q = -\lambda_g(T) \cdot \varphi / m;$$

Heat release in the reaction layer of the condensed phase (or on the burning surface) Q is as follows:

$$Q = c \cdot (T_s - T_o) - q - q_r + q_m;$$

Where q_r is the radiant heat supply from flame into solid and q_m is heat of nitramine melting.

It was assumed that heat of HMX's melting is equal to 24 cal/g (per gramm of HMX) and that of RDX is equal to 29 cal/g (per gramm of RDX). That implies that q_m=19.2 cal/g for HMX's containing mixtures and q_m=23.2 cal/g for RDX's containing mixtures.

The radiant heat supply was estimated by formula: $q_r = k_o \cdot k_1 \cdot T_f^4 / m$, where k_o is the coefficient of the burning surface absorption of the flame radiation and $\cdot k_1$ is the degree of the flame blackness. It

was assumed that k_o=0.5, k_1=0.1. It can be seen that at low pressures a significant radiant heat supply from gas into solid is observed: q_r=(10.4-15) cal/g at 5 atm. However it decreases quickly when pressure increases - at 100 atm q_r is equal to 2-3 cal/g. Tables 1-4 show that values of q_r can significantly decrease at low pressures when T_o increases.

Temperature gradient φ in gas close to the burning surface increases with pressure. It has very large values and can be as much as $1.4 \cdot 10^5$ K/cm. However heat feedback from gas into solid by heat conduction is relatively small because of very low values of λ_g. Tables 1-4 show that q decreases when pressure increases - q is equal to 64-42 cal/g at 5 atm and to 18-26 cal/g at 100 atm. Values of q change insignificantly with T_o variations.

Heat release in solid Q increases with pressure. It has significant values - 65-98 cal/g at 5 atm and 179-195 cal/g at 100 atm. It is important to stress that Q increases with burning rate. Tables 1-4 show that at constant pressures values of Q significantly increases when T_o decreases. It can be explained by the necessaty of a large heat consumption for the solid heating at low sample temperatures.

Table 4: Burning wave parameters of mixture 4 ([BAMO-AMMO]/RDX)

No	p, atm	5	10	20	50	80	100
	T_o, °C	20	-100/20/90	-100/20/90	-100/20/90	-100/20/90	-100/20
1	m, g/cm²s	0.12	0.17/0.22/ 0.27	0.33/0.42/ 0.49	0.75/0.87/ 1.02	1.1/1.27/ 1.47	1.3/1.5
2	T_s, °C	335	350/370/380	390/410/420	460/470/480	480/490/500	495/500
3	$\varphi \cdot 10^{-4}$, K/cm	2.5	3.6/3.5/5.0	6.0/5.0/7.0	9.5/8.5/12	10.5/10.5/14	11/11
4	q, cal/g	42	46.6/36.6/42.6	41.8/28.6/34.3	31.6/24.4/30.6	25/22/25	22/19
5	q_r, cal/g	10.4	9/8/8	6.5/6/6	3.4/3.4/3.4	2.4/2.5/2.3	2.0/2.1
6	Q, cal/g	98	148/118/89	171/145/115	212/175/145	228/187/160	237/194
7	l, μm	156	118/107/106	90/80/74	63/57/33	50/47/43	48/44
8	l_m, μm	90	60/80/100	45/65/70	40/50/60	40/40/40	30/44
9	$\chi \cdot 10^3$, cm²/s	1.2	1.3/1.4/1.8	1.9/2.2/2.3	2.9/3.1/3.5	3.5/3.9/4.2	3.9/4.2
10	$\lambda_s \cdot 10^4$, cal/cm·s·K	7.5	8.1/8.7/11.2	11.8/13.7/14	18/19.3/21.8	21.8/24/26	24.3/26
11	T_1, °C	950	-/1000/1080	-/-/-	-/-/-	-/-/-	-/-
12	T_f, °C	1800	1900/2000/ 2100	2100/2200/ 2300	2200/2300/ 2400	2230/2330 2400	2230/ 2330
13	L_1, μm	800	-/450/600	-/-/-	-/-/-	-/-/-	-/-
14	L, mm	2.5	1.0/2.0/2.5	1.5/2.0/2.0	1.5/1.5/1.5	1.2/1.3/1.3	1.0/1.0
15	ϑ, μm	40	32/25/20	17/14/12	8.0/6.8/6.0	5.6/4.8/4.2	4.7/4.1
16	$\lambda_g \cdot 10^4$, cal/cm·s·K	2.0	2.2/2.3/2.3	2.3/2.4/2.4	2.5/2.5/2.6	2.6/2.6/2.6	2.6/2.6
17	Φ_o, kcal/cm³s	1.2	2.5/3.2/5.7	8.3/8.8/14.4	30/31.4/52	49/56.7/87.5	60.8/70

4.1.7. *Heat release rate in gas close to the burning surface.*

Heat release rates Φ_o in gas close to the surface was estimated by the use of the obtained data. Φ_o shows, obviously, the intensity of chemical reactions in gas. Values of Φ_o were obtained from the heat conduction equation and the temperature profiles. The heat conduction equation connected with the burning surface for the gas phase of stable propagated combustion wave is as follows:

$$d/dx\cdot(\lambda_g dT/dx)-m\cdot c_p\cdot dT/dx+\Phi(x)=0;$$

Here $\Phi(x)$ is the distribution of the heat release rate in the gas phase of the combustion wave. The first term of the equation at $x\approx 0$ is small and thus the following approximately expression for $\Phi(x\approx 0)=\Phi_o$ is valid:

$$\Phi_o=c_p\cdot m\cdot\varphi;$$

Tables 1-4 show that the values Φ_o increase with pressure from (0.5-0.8)·kcal/cm^{3}s at 2 atm up to (34-65) ·kcal/cm^{3}s at 100 atm.

4.2. Burning Rate Control Regions.

The results of measurements of $q+q_r$ and Q and the investigations of the gas phase zone behaviour show that burning rate of mixtures 1-4 are caused by the heat release in solid (or on solid surface) and, in a smaller degree, by the heat feedback from the gas layer which is close to the surface. It was mentioned above also that the values of of $q+q_r$ decreases when the burning rate increases. An important conclusion can be made from the analysis of the obtained data: the high temperature region of the burning waves cannot affect the burning rate. The influence of the heat release in the gas phase on the burning rate can be estimated by the following formula obtained as a solution of the heat conduction equation:

$$m\cdot q=\int_0^\infty \Phi\cdot\exp(-x/\vartheta)\cdot dx; \qquad (1.5)$$

This formula shows that influence of heat release in gas on m decreases very quickly when $x>\vartheta$. Tables 1-4 show that values ϑ are small and they are significantly smaller than gas zone sizes L and L_1. Indeed, values of ϑ are equal to 50-4 μm, but L_1 are equal to 200-900 μm and L are equal to 2.5 -1 mm. The data imply that high temperature region of the burning waves cannot affect the burning rate.

Thus the obtained results show that the burning rate control regions in the combustion waves for all regimes of the mixture combustion are the regions of heat release in solid just under the burning surface (or immediately on the burning surface) and thin low-temperature gas layers close to the burning surface. High temperature gas regions cannot influence the burning rate in fact because of a very large heat resistance of the gas phase of the mixtures.

4.3. Macrokinetics of Solid Gasification.

The following equation connects burning rate of solid with burn-surface temperature and macrokinetic characteristics of solid gasification:

$$m^2=\lambda_s\rho/Q^2\cdot\Re T_s^2/E\cdot k_o Q^*\cdot 1/N\cdot\exp(-E/\Re T_s);$$

where $N=1/\eta_s+(1-\eta_s)/\eta_s\cdot\ln(1-\eta_s)-(q/Q)\cdot[\ln(1-\eta_s)]/\eta_s$; $\eta_s=Q/Q^*$; Q^* is the maximum of the heat release in solid E is activation energy of limiting stage of the gasification process, T_s in K. For studied combustion waves $N\cong 1$. The expression was obtained by solution of system of two equations for the steady propagated burning wave - the heat conduction equation for solid phase and the equation of diffusion of reagents. The burning wave propagates due to heat release in solid Q and heat feedback from gas to solid q. Function of the volumetric heat release rate Φ_s in solid was assumed as follows:

$$\Phi_s(\eta, T)=Q^* k_o\cdot\rho\cdot(1-\eta)\cdot\exp(-E/\Re T);$$

Here η is the reaction completeness ($\eta=\eta_s$ on the burning surface), k_o is the preexponent multiplier.

The member $\exp(-E/\Re T_s)$ plays the most important role in this formula. Because of that the connection m and T_s can be presented by the following simplified expression:

$$m=A\cdot\exp(-E/2\Re T_s);$$

This expression has been designated "gasification law". The results of measurement, presented in Tables 1-4, allow the following gasification laws for mixtures 1-4 to be obtained:

$m=3.8\cdot10^3\cdot\exp(-25000/2\Re T_s)$; (m in g/cm^{2}s, T in K), at $T_s<470°C$

$m=1.7\cdot10^6\cdot\exp(-43000/2\Re T_s)$; (m in g/cm^{2}s, T in K), at $T_s>470°C$

The obtained values of activation energy of the gasification process and the point of E changing ($T_s^*=470°C$) are very close to those of cyclic nitramines. Possibly, gasification of oxidizers (HMX and RDX) in the reaction layer of burning mixtures 1-4 is the limiting stage of the process of the mixture gasification.

4.4. Pressure and Temperature Sensitivities for m and T_s. Criteria of Stable Combustion.

The following pressure and temperature sensitivities for burning rate and burning surface temperature were found from the data presented on Tables 1-4 ($T_o=20°C$):

$\beta=(\partial\ln m/\partial T_o)_{p\text{-const}}$, - temperature sensitivity of mass burning rate;

$r=(\partial T_s/\partial T_o)_{p\text{-const}}$, - temperature sensitivity of burning surface temperature;

$\nu=(\partial\ln m/\partial\ln p)_{To\text{-const}}$, - pressure sensitivity of mass burning rate;

$\mu=(T_s-T_o)^{-1}\cdot(\partial T_s/\partial\ln p)_{To\text{-const}}$, - pressure sensitivity of burning surface temperature;

The obtained results are shown in Tables 5 and 6. Criteria of stable combustion - Zeldovich criterion $k=\beta\cdot(T_s-T_o)$ and Novozilov criterion $k^*=(k-1)^2/(k+1)r$ - are presented also in Table 5 and 6. Criterion k^* is necessary to calculate only for regimes having values of $k>1$. Combustion is stable if $k^*<1$. Tables 5 and 6 show that mixtures 1-4 have stable combustion at $T_o=20°C$.

At $T_o=-100°C$ exist regimes when $k>1$, however for these regimes always $k^*<<1$.

At $T_o=90°C$ always $k<1$. Thus mixtures 1-4 have stable combustion under investigated conditions.

Table 5: Sensitivities of burning rate and surface temperature and criteria of stable combustion of mixtures 1 and 2 at $T_o=20°C$ (presented as fractions: mix.1/mix.2)

p, atm	10	20	50	80	100
ν	0.83/0.92	0.80/0.84	0.76/0.80	0.76/0.80	0.76/0.80
r	0.17/0.19	0.155/0.20	0.13/0.15	0.10/0.105	0.09/0.083
μ	0.172/0.163	0.171/0.179	0.115/0.111	0.104/0.110	0.092/0.092
k	0.97/1.01	0.87/0.924	0.79/0.94	0.79/1.038	0.8/0.96
k^*	-/0.0003	-/-	-/-	-/0.008	-/-

Table 6: Sensitivities of burning rate and surface temperature and criteria of stable combustion of mixtures 3 and 4 at T_o=20°C (presented as fractions: mix.3/mix.4)

p, atm	10	20	50	80	100
ν	0.90/0.95	0.82/0.84	0.80/0.80	0.79/0.78	0.79/0.78
r	0.19/0.16	0.16/0.16	0.12/0.12	0.066/0.12	0.067/0.04
μ	0.174/0.163	0.168/0.172	0.098/0.098	0.094/0.094	0.092/0.092
k	0.95/0.81	0.76/0.78	0.72/0.81	0.61/0.7	0.576/0.576
k*	-/-	-/-	-/-	-/-	-/-

4.5. Pressure-Driven Burning-Rate Response Functions.

It is interesting to investigate burning rate behaviour of mixtures 1-4 under conditions of oscillatory pressure. Let us assume that $p=p_o+p_1\cdot\cos\varpi t$, where $p_1<<p_o$ and ϖ is cyclic frequency of oscillation in 1/s. Then nondimensional burning rate is equal to $V=1+V_1\cdot\cos\varpi t$, where $V=r_b/r_{bo}$, $V_1=r_b^{\sim}/r_{bo}$; r_{bo} is a stationary burning rate and $r_b^{\sim}$. It is convenient to analyse burning rate response in complex form. In this case complex nondimensional burning rate is equal to $V=1+V_1\cdot e^{-i\omega t}$ and complex nondimensional pressure is equal to $\eta=1+\eta_1\cdot e^{-i\omega t}$, where $\eta_1=p_1/p_o$, and ω is nondimensional frequency.

The following expression for burning rate response function to oscillatory pressure takes place:

$$U=[\nu+(\nu\cdot r-\mu\cdot k)\cdot(z-1)]/[1+r\cdot(z-1)-k\cdot(z-1)/z];$$

Here $z=(1+\sqrt{1+4i\omega}\,)/2$; $U=V_1/\eta_1$, V_1 is nondimensional burning rate complex amplitude, and ω is nondimensional frequency which is equal to the cyclic frequency ϖ, in 1/s, multiplied by the time of solid heat layer relaxation χ/r_b^2. Values of ν, μ, k and r here are based on the mean pressure p_o and because of that data from Tables 5, 6 can be used for estimations of complex functions of U. Thus, indeed, we can investigate burning rate behaviour of mixtures 1-4 under conditions of pulsating pressure.

Results of calculationsof dimensionless amplitudes Re{U} and phase Im{U} of the response as functions of ω are shown on Figs. 19-22 (T_o=20°C). Response functions of mixtures 1-4 are close each other and because of that Figs. 19-22 show functions of Re{U(ω)} and Im{U(ω)} only for mixture 1. Figures 19-22 show that $Re\{U\}_{max}$ are equal to 1.3-1.5 and practically independent on pressure. Resonance frequencies ω_n are equal approximately to 3.5 at 10 and 20 atm, to 4.5 at 50 atm and to 6.5 at 100 atm. It is natural that function Im{U(ω)}, presenting the phase of response functions, changes the sign at the resonance frequency. Functions of Re{U(ω)} weakly depend on ω, especially at elevated p. The result shows that resonance phenomena in burning mixtures 1-4 are significantly depressed due to viscous behaviour of the oscillations. In fact, the pulsating combustion of the mixtures is an example of a relatively smoothed resonance phenomenon. Such behaviour must be attributed to large amount of cyclic nitramines in the mixtures, because these nitramines have decreased $Re\{U\}_{max}$ and weak dependence Re{U(ω)}.

5. Results of Measurements and Processing for Mixtures 5-8.

The characteristics of the initial mixtures were as follows:
5) GAP1U/HMX, density ρ=1,38 g/cm^3; sum formula: $O_{23.6}H_{31.7}N_{27.6}C_{16.9}$; T_{ad}=2695 K;
6) GAP1U/RDX, density ρ=1,19 g/cm^3; sum formula: $O_{23.6}H_{31.7}N_{27.66}C_{16.86}$; T_{ad}=2705 K;
7)(BAMO-THF)/HMX, density ρ=1,70 g/cm^3; sum formula: $O_{23.3}H_{34.9}N_{26.6}C_{18.3}$; T_{ad}=2465 K;
8) (BAMO-THF)/RDX, density ρ=1,65 g/cm^3; sum formula: $O_{23.4}H_{33.9}N_{26.1}C_{18.7}$; T_{ad}=2445 K;
Binder (BAMO-THF) have proportion 50:50. Cylindrical samples of 8 mm in diameter and 2 cm in length were burned in a bomb of constant pressure. Temperature profiles and surface temperatures were obtained for the indicated mixtures at pressures 10-100 atm and at sample temperature T_o=+20C°. Carbon residue on the burning surface of the mixtures did not observed. Temperature profiles were received and after averaging they were analysed. Tables 7, 8 show the obtained characteristics. The nominations are the same as in Tables 1-4.

5.1. Burning Wave Characteristics.

5.1.1. *Mass burning rate.* Mass burning rate m increases for mixtures 5-8 when pressure increases. Values of m for mixtures 5-7 are close each other and that for mixture 8 is less, especially at elevated pressures. At 2 atm m are equal to 0.06-0.08 g/cm^{2}s, at 10 atm - 0.17-0.22 g/cm^{2}s, at 20 atm - 0.3-0.45 g/cm^{2}s. At elevated pressures diapason of values m increases: at 50 atm - 0.8-0.82 g/cm^{2}s for mixtures 6 and 7, but for mixture 8 - 0.45 g/cm^{2}s; at 100 atm - 1.38-1.65 g/cm^{2}s for mixtures 6 and 7, but for mixture 8 - 1.09 g/cm^{2}s.
5.1.2. *Burning surface temperature.* Burning surface temperature T_s always increases when m and pressure increase. Values of T_s changes significantly: from 280-360°C at 2 atm up to 560-580°C at 100 atm.
5.1.3. *Geometric structure of the temperature profiles in gas.* The gas phase has two-zone structure: the first zone with mean zone temperatures T_1 and the flame zone with the final zone temperatures T_f. Both zones merge at 20-50 atm. Only the first zone exists at 2 atm for mixture 6 with the final zone temperature T_1. Values of T_1 are equal to 900-1100°C. Thermodynamically calculated values of T_f are achieved at 20-50 atm. Distances L_1 between the burning surface and the beginning of the flame zone at pressures 2 (10)-20 atm are very small for mixtures 5, 6 (250-100 μm) and very large for mixtures 7, 8 (0.7-1.5 mm). Distances L between the burning surface and the flame - 1.5 - 0.8 mm for mixtures 5, 6 and 3.5 - 1.0 mm for mixtures7, 8.
5.1.4. *Characteristic sizes in gas and solid.* Mixtures 5, 6 have l =210-30 μm and mixtures 7, 8 - l =65-20 μm. Conductive sizes ϑ of the gas phase decrease when pressure increases and comprise 23-3 μm for mixtures 7, 8 and 85-4.8 μm for mixtures 5, 6. It is obvious that $\vartheta << L_1$.
5.1.5. *Heat diffusivity and heat conductivity of heat layer in solid.* Values χ increase from (1-1.5)·10^{-3} cm^2/s at low pressures up to (3-3.5)·10^{-3} cm^2/s at 100 atm. That are normal values of χ for many propellant mixtures. The solid heat conductivity was obtained by formula $\lambda_s=\chi\cdot c\cdot\rho$; it was assumed that solid specific heat c=0.4 cal/g·K. Tables 7, 8 show that λ_s increases, when pressure increases, from 5·10^{-4} cal/cm·s·K at 2 atm up to (16-23)·10^{-4} cal/cm·s·K at 100 atm.
5.1.6. *Heat release in solid and heat feedback from gas to solid.* The radiant heat supply was estimated by formula: $q_r=k_o\cdot k_1\cdot T_f^4/m$, where k_o is coefficient of the burning surface absorption of the radiation and $\cdot k_1$ is degree of the flame blackness. That was assumed that k_o=0.5, k_1=0.1. It can be seen that at low pressures a significant radiant heat supply from gas into solid is observed. Tables 7, 8 show that the temperature gradient φ in gas close to the burning surface has very large values: it can be as much as 10^5 K/cm. Values of q and Q are comparable at 2-5 atm. But at elevated pressures values Q are more than values of q. As a rule, Q increases with pressure, however q, as a rule, decreases.

5.1.7. *Heat release rate in gas close to the burning surface.* Tables 7, 8 show that values of Φ_o increase with pressure from (0.5-0.8)·kcal/cm^{3}s at 2 atm up to (34-65) ·kcal/cm^{3}s at 100 atm.

Table 7: Burning wave parameters of mixtures 5 and 6 at T_o=20°C
(indicated as fractions: mix.5/mix.6)

p, atm	2	5	10	20	50	100
r_b, cm/s	0.06/0.047	0.107/0.126	0.17/0.22	0.30/0.38	0.58/-	1.0/-
m, g/cm^{2}s	0.083/0.056	0.148/0.15	0.235/0.27	0.42/0.455	0.8/-	1.38/-
T_s, °C	360/280	400/370	440/440	490/460	560/-	580/-
$\varphi \cdot 10^{-4}$, K/cm	2.3/2.0	4.5/3.5	5.0/4.5	6.5/6.0	10/-	11/-
q, cal/g	55/68	70/49	51/40	39/32	34/-	22/-
Q, cal/g	74/41	84/100	124/142	162/161	198/-	219/-
l, μm	170/210	110/80	90/70	60/45	35/-	30/-
T_1, °C	950/900	1000/1000	1050/1100	1100/-	-/-	-/-
T_f, °C	2100/1700	2200/2100	2250/2200	2300/2300	2400/-	2420/-
L_1, μm	250/-	150/230	120/180	100/-	-/-	-/-
L, mm	1.5/1.5	1.0/1.2	1.0/1.0	1.2/0.9	0.8/-	0.8/-
ϑ, μm	63/85	84/35	24/21	14/13	8/-	4.8/-
$\chi \cdot 10^3$, cm^2/s	1/1	1.2/1.2	1.5/1.5	1.8/2.0	2/-	3/-
l_m, μm	60/100	50/60	40/55	35/40	30/-	25/-
q_r, cal/g	26/18	17/14	12/9	7/6.5	4/-	2/-
$\lambda_s \cdot 10^4$, cal/cm·s·K	5.5/4.8	6.6/5.8	8.3/7.2	9.9/9.6	11/-	16.5/-
$\lambda_g \cdot 10^4$, cal/cm·s·K	2/1.9	2.3/2.1	2.4/2.4	2.5/2.4	2.7/-	2.8/-
Φ_o, kcal/cm^{3}s	0.8/0.47	2.8/2.2	4.9/5.1	11.5/11.5	34.0/-	64.5/-

5.2. Burning Rate Control Regions.

The results of measurements of $q+q_r$ and Q and the investigations of the gas phase zone behaviour show that burning rate of mixtures 5-8 are caused by the heat release in solid (or on solid surface) and, in a smaller degree, by the heat feedback from the gas layer which is close to the surface. An important conclusion can be made from the analysis of the obtained data: the high temperature region of the burning waves cannot affect the burning rate. The same analysis as in the previous case show that high temperature region of the burning waves cannot affect the burning rate. Thus the obtained results show that the burning rate control regions in the combustion waves for all regimes of the mixture combustion are the regions of heat release in solid just under the burning surface (or immediately on the burning surface) and thin low-temperature gas layers close to the burning surface. High temperature gas regions cannot influence the burning rate in fact because of a very large heat resistance of the gas phase of the mixtures.

Table 8: Burning wave parameters of mixtures 7 and 8 at T_o=20°C
(indicated as fractions: mix.7/mix.8)

p, atm	10	20	50	100
r_b, cm/s	0.11/0.14	0.18/0.2	0.26/0.5	0.64/1.0
m, g/cm^{2}s	0.187/0.23	0.306/0.33	0.45/82	1.09/1.65
T_s, °C	380/400	420/450	450/470	500/520
$\varphi \cdot 10^{-4}$, K/cm	2.8/2.5	3.0/4.0	6.5/7.3	7.5/7.5
q, cal/g	27/19.6	17.6/23	27.4/17	13.8/9
Q, cal/g	128/148	156/166	158/183	195/213
l, μm	64/65	65/70	56/37	32/20
T_1, °C	950/1000	1000/1100	-/-	-/-
T_f, °C	1880/2000	1950/2100	2200/2170	2200/2170
L_1, mm	1.5/1.0	0.8/0.7	-/-	-/-
L, mm	3.5/2.5	2.5/1.5	2.0/2.0	1.0/1.5
ϑ, μm	23/19	14/14	10/5.5	4.3/3.0
$\chi \cdot 10^3$, cm^2/s	1.2/1.5	2.0/2.3	2.5/3.0	3.5/3.5
l_m, μm	30/50	55/60	40/30	20/20
q_r, cal/g	7.8/7.9	5.5/6.5	5.6/2.9	2.3/1.5
$\lambda_s \cdot 10^4$, cal/cm·s·K	8.2/9.5	13.6/15.2	17/19.8	23.8/23.0
$\lambda_g \cdot 10^4$, cal/cm·s·K	1.8/1.8	1.8/1.9	1.9/1.9	2.0/2.0
Φ_o, kcal/cm^{3}s	2.2/2.4	3.8/5.5	12.3/26.2	34.6/52.6

6. Conclusions About Combustion Mechanisms of Nitramine/Polymer Mixtures.

Nitramine/Energetic Polymer Binders.

1) The mixtures 1-8 have large heat release in solid Q, which increases with pressure and burning rate m. Heat feedback from gas to solid is less (than Q) and decreases when p and m increase. At low pressures a significant role in the heat feedback from gas to solid plays radiant heat flux from flame to solid.

2) Burning rate control regions are located on solid surface (due to large heat release in solid) and in thin low-temperature gas layer close to the burning surface.

3) Process of oxidizer decomposition plays the limiting role in the mixtures gasification, because macrokinetics of the mixture gasification are very close to those of HMX and RDX.

4) The gas phase of burning mixtures has two-zone structure at low pressures (5-10 atm), which merges into one zone when pressure increases. Increasing initial temperature can create two-zone

structure from one zone and decreasing initial temperature can merge the two-zone structure into one zone.

5) Thickness L of the reacting gas zone is equal to 1-2.5 mm. As a rule, L decreases when pressure increases (especially in region 50-100 atm) and increases with the initial temperature.

6) Completeness of combustion is achieved at 50-80 atm. Flame temperature increases with the initial temperature.

7) Stable combustion is observed under investigated conditions.

8) Pressure-driven burn-rate response functions of the investigated mistures have viscous behaviour, without charp increase of burning rate response amplitude close to resonance frequency.

Comparison of Combustion Mechanisms of Mixtures based on Energetic Binders and Mixtures based on HTPB.

1) Mixtures based on HTPB have decreased burning rate, burning surface temperature, heat release in solid and heat feedback from gas to solid, than, under comparible conditions (pressure, initial temperature), mixtures based on energetic binders.

2) Mixtures based on HTPB have increased thickness of reacting gas zone. Two-zone structures in the gas phase are observed up to higher pressures than two-zone structures of mixtures based on energetic binders.

3) Mixtures based on HTPB have decreased flame temperatures.

4) Mixtures based on HTPB and on energetic binders have similar macrokinetics of solid gasification, and similar positions of burning rate control regions.

FIGURES

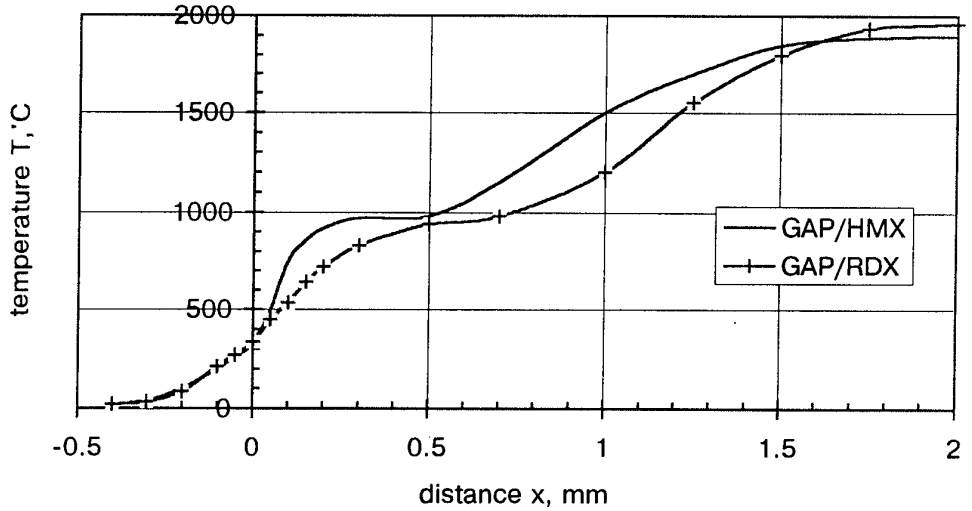

Figure 1: Averaged temperature profiles T(x) of mixtures 1 (GAP2/HMX) and 2 (GAP2/RDX) at 5 atm, To=20°C.

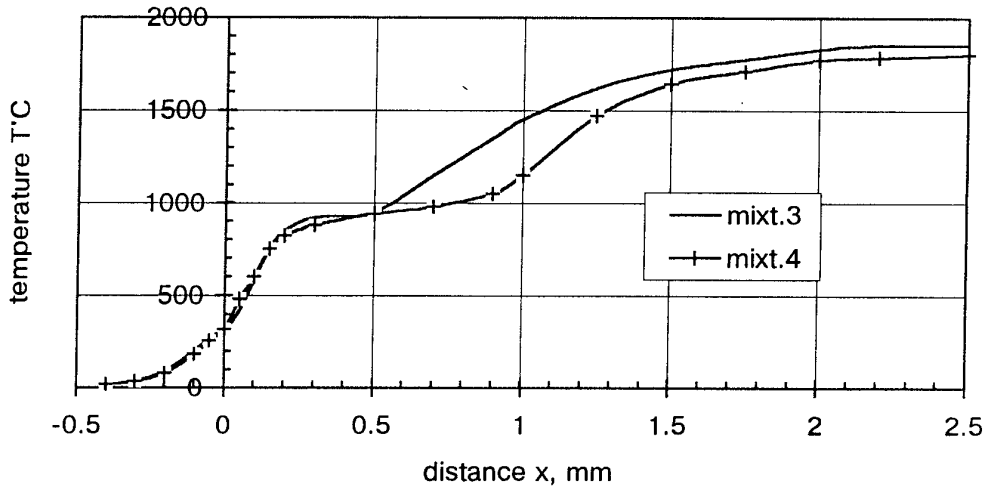

Figure 2: Averaged temperature profiles T(x) of mixtures 3 ([BAMO-AMMO]/HMX) and 4 ([BAMO-AMMO]/RDX) at 5 atm, To=20°C.

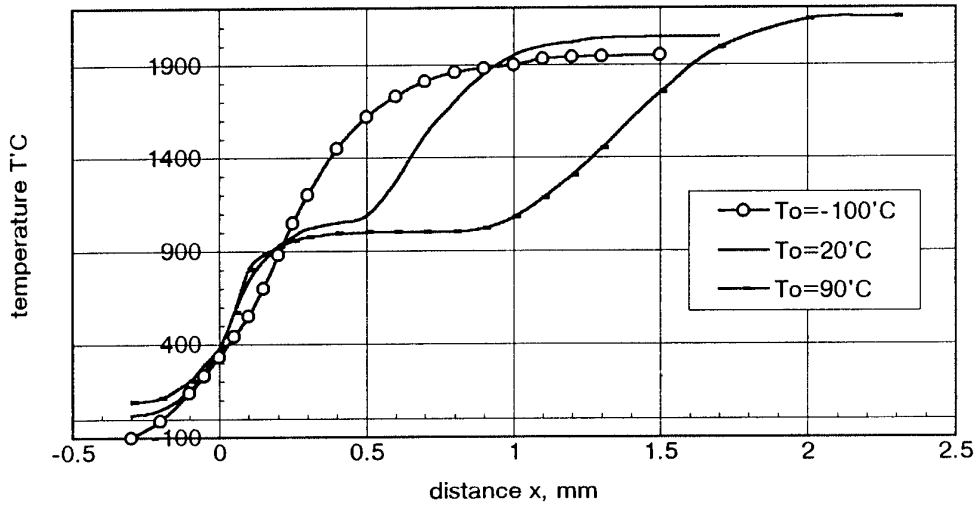

Figure 3: Averaged temperature profiles T(x) of mixture 1 (GAP2/HMX) at 10 atm and different To.

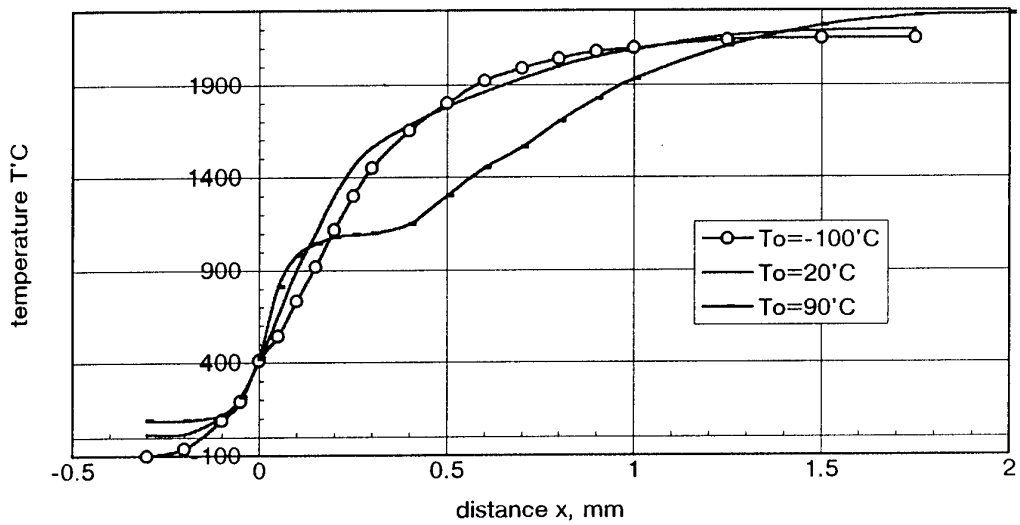

Figure 4: Averaged temperature profiles T(x) of mixture 1 (GAP2/HMX) at 20 atm and different To.

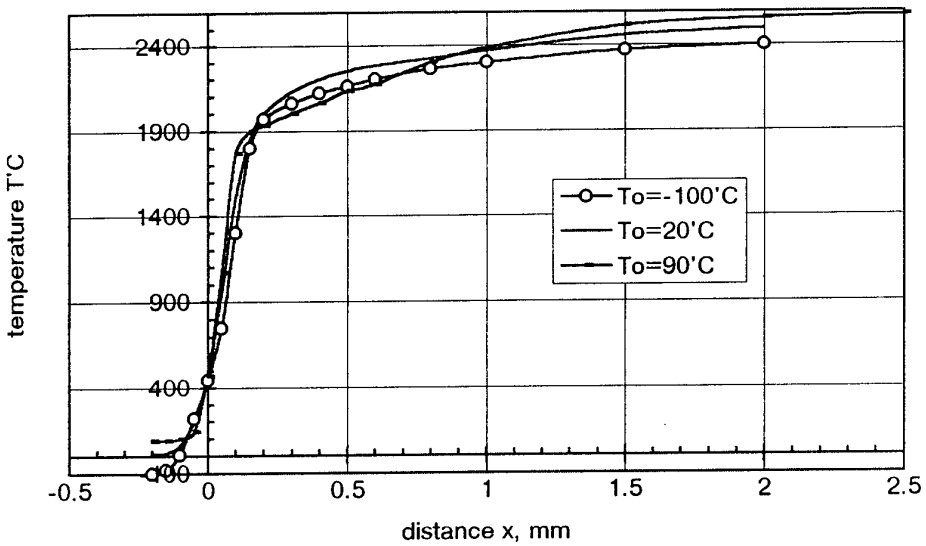

Figure 5: Averaged temperature profiles T(x) of mixture 1 (GAP2/HMX) at 50 atm and different To.

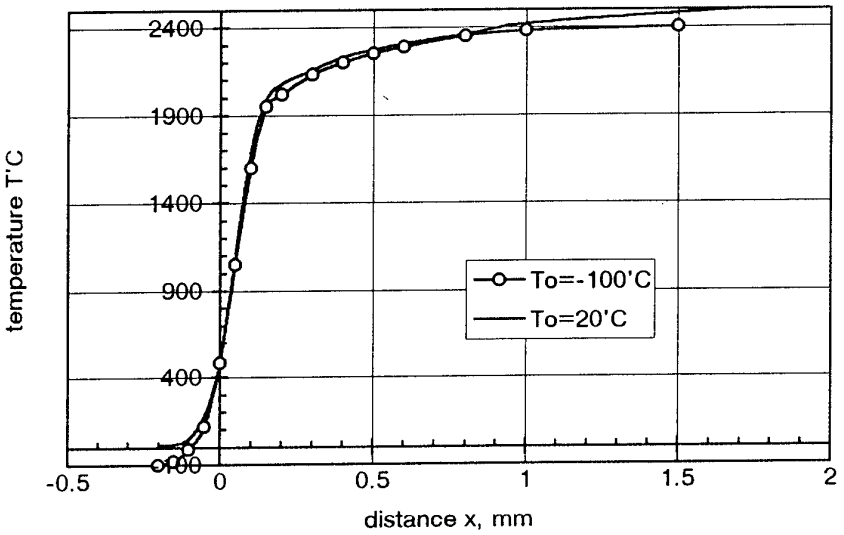

Figure 6: Averaged temperature profiles T(x) of mixture 1 (GAP2/HMX) at 100 atm and different To.

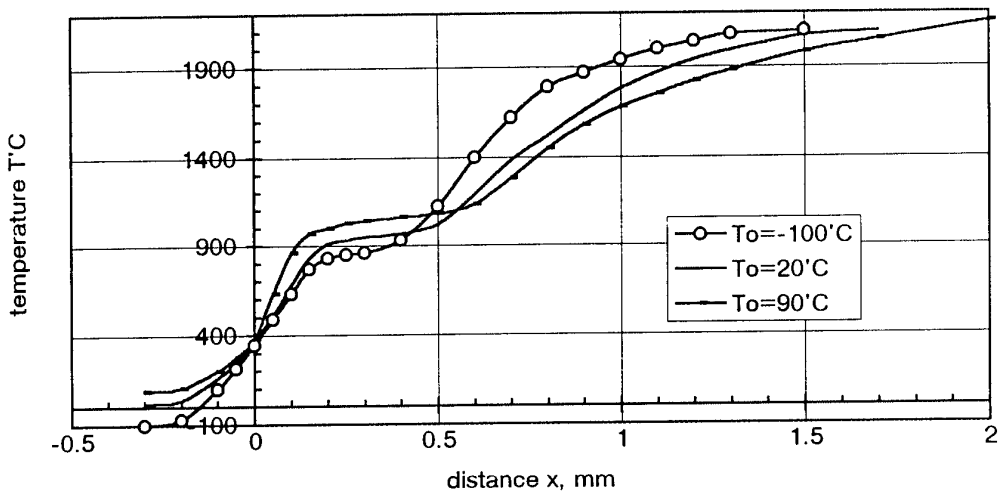

Figure 7: Averaged temperature profiles T(x) of mixture 2 (GAP2/RDX) at 10 atm and different To.

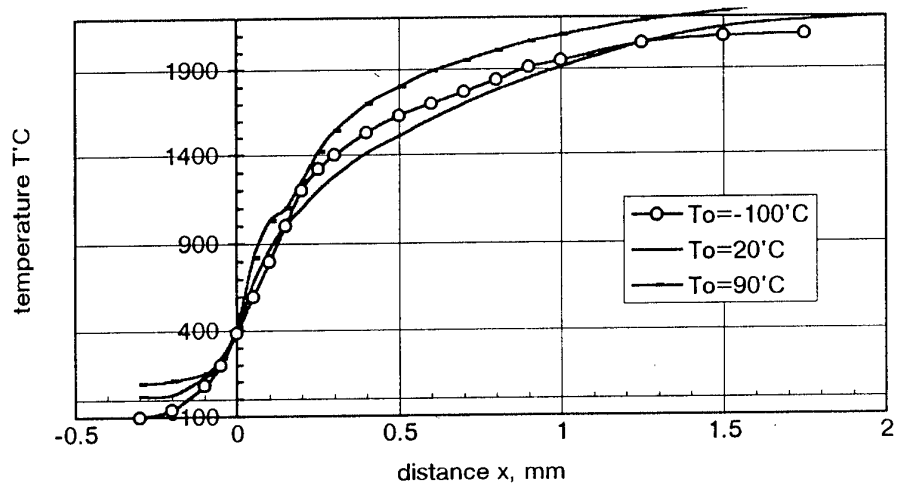

Figure 8: Averaged temperature profiles T(x) of mixture 2 (GAP2/RDX) at 20 atm and different To.

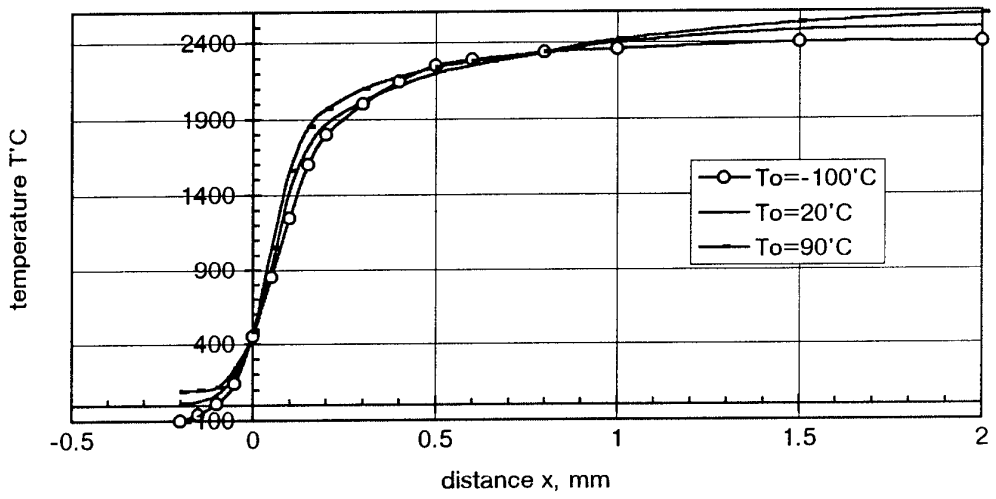

Figure 9: Averaged temperature profiles T(x) of mixture 2 (GAP2/RDX) at 50 atm and different To.

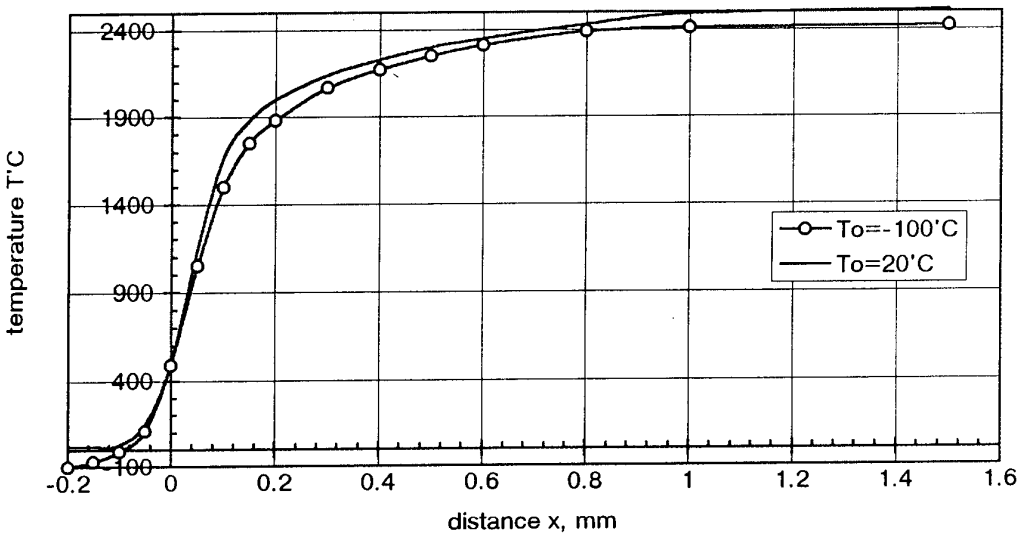

Figure 10: Averaged temperature profiles T(x) of mixture 2 (GAP2/RDX) at 100 atm and different To.

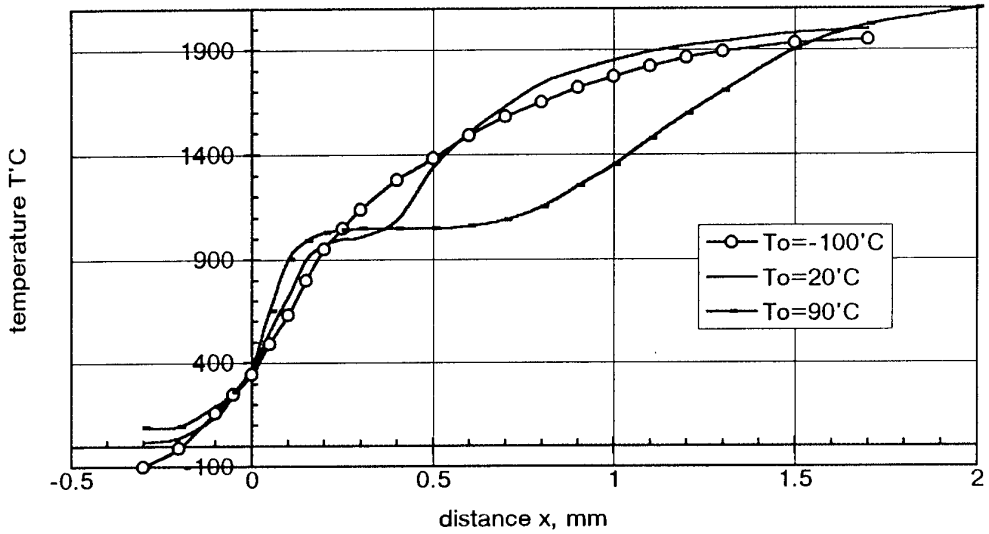

Figure 11: Averaged temperature profiles T(x) of mixture 3 [(BAMO-AMMO)/HMX] at 10 atm and different To.

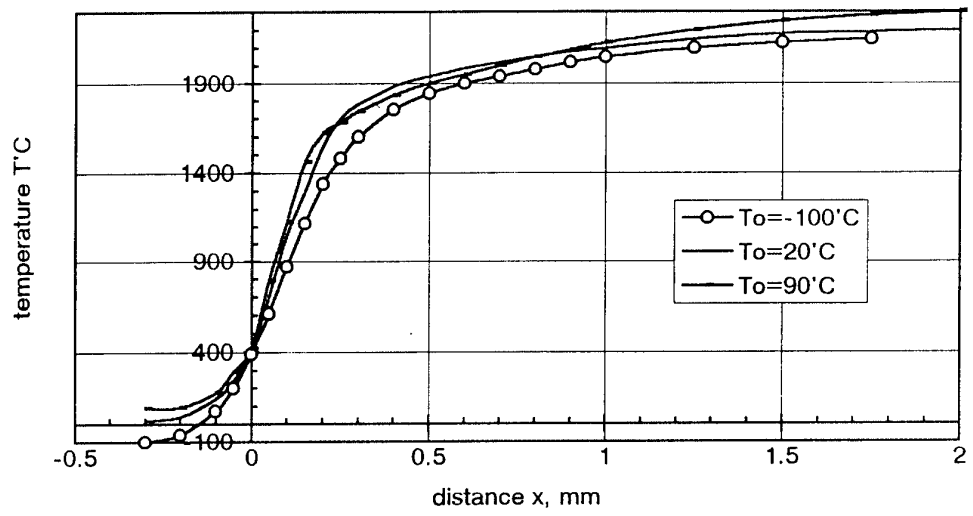

Figure 12: Averaged temperature profiles T(x) of mixture 3 [(BAMO-AMMO)/HMX] at 20 atm and different To.

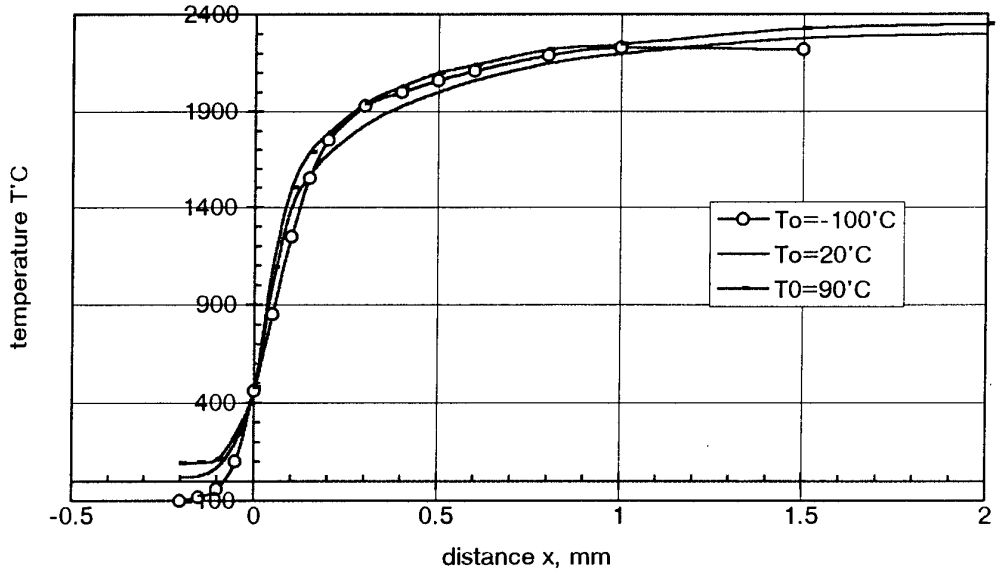

Figure 13: Averaged temperature profiles T(x) of mixture 3 [(BAMO-AMMO)/HMX] at 50 atm and different To.

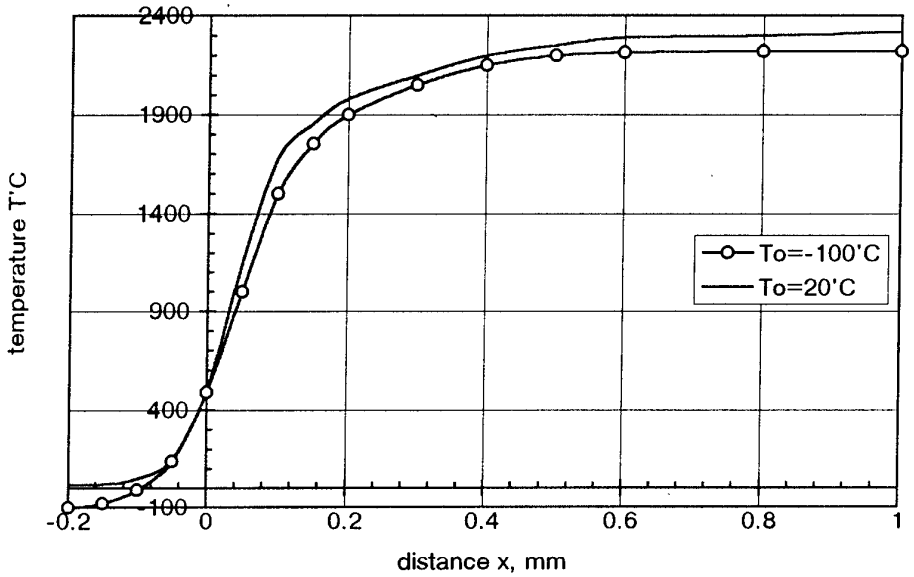

Figure 14: Averaged temperature profiles T(x) of mixture 3 [(BAMO-AMMO)/HMX] at 100 atm and different To.

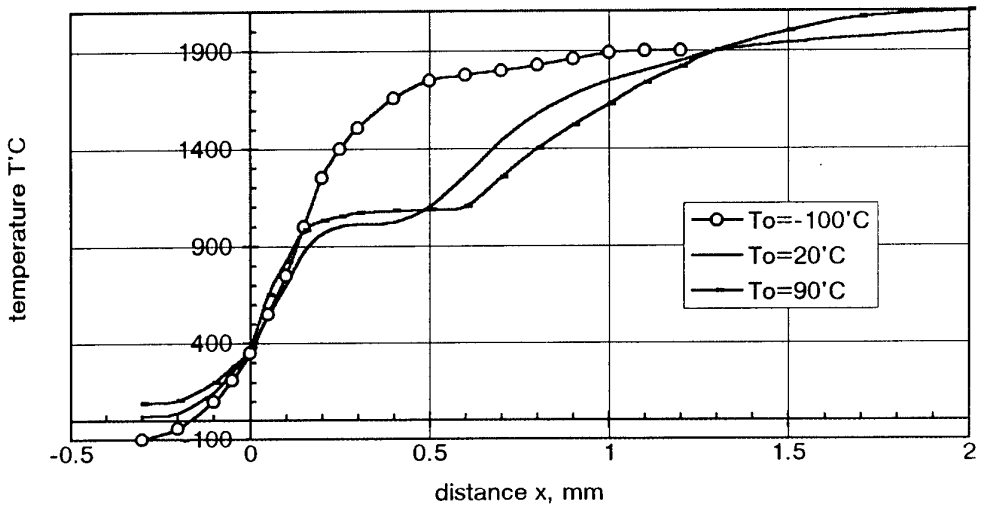

Figure 15: Averaged temperature profiles T(x) of mixture 4 [(BAMO-AMMO)/RDX] at 10 atm and different To.

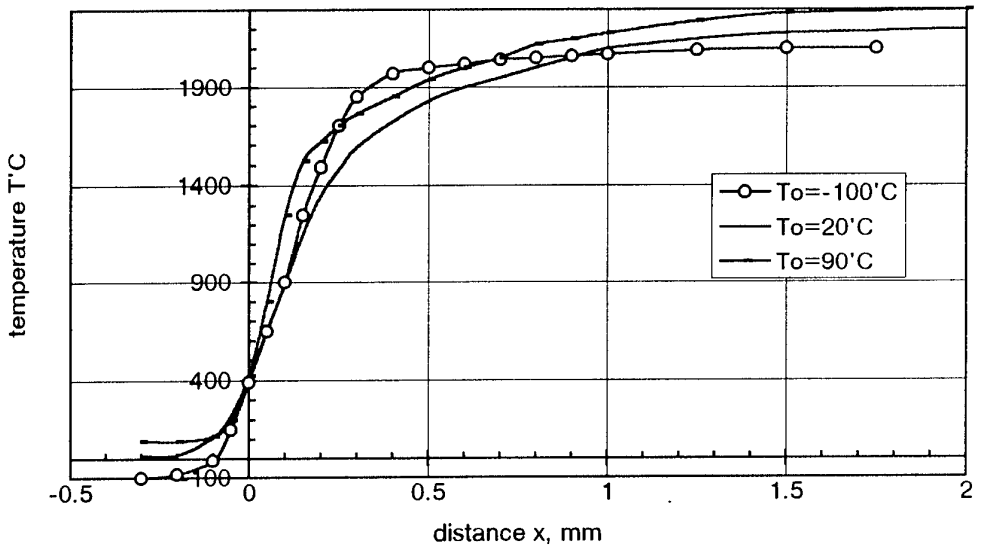

Figure 16: Averaged temperature profiles T(x) of mixture 4 [(BAMO-AMMO)/RDX] at 20 atm and different To.

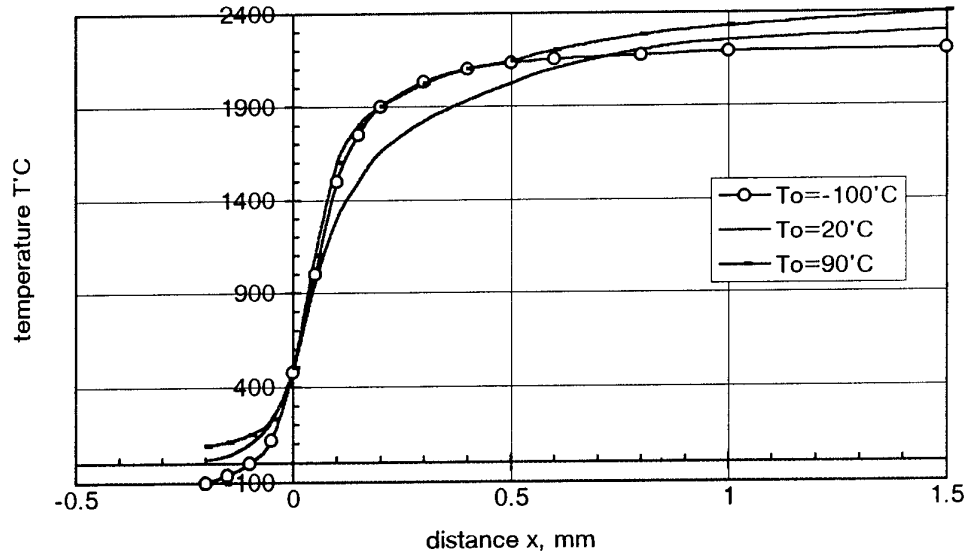

Figure 17: Averaged temperature profiles T(x) of mixture 4 [(BAMO-AMMO)/RDX] at 50 atm and different To.

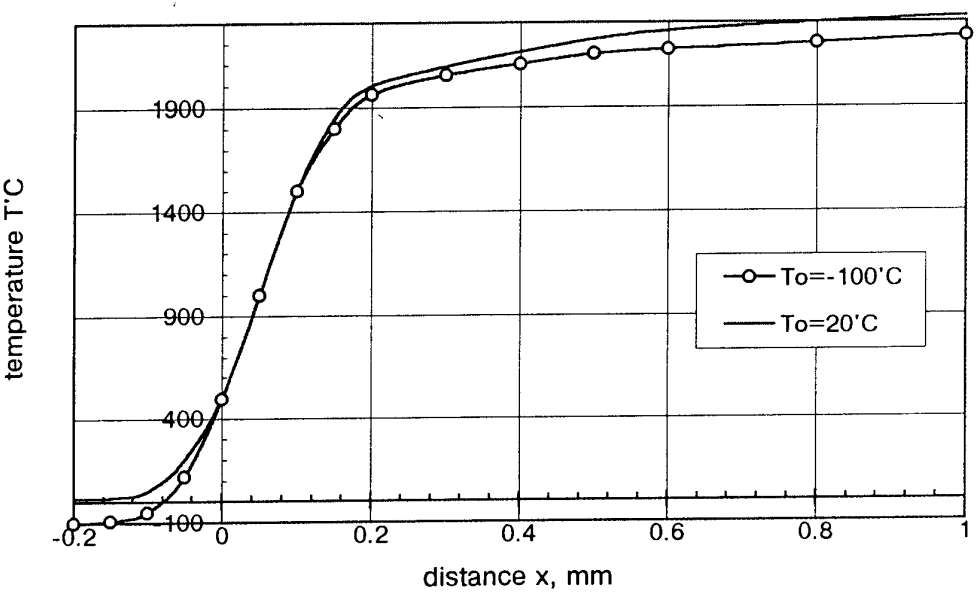

Figure 18: Averaged temperature profiles T(x) of mixture 4 [(BAMO-AMMO)/RDX] at 100 atm and different To.

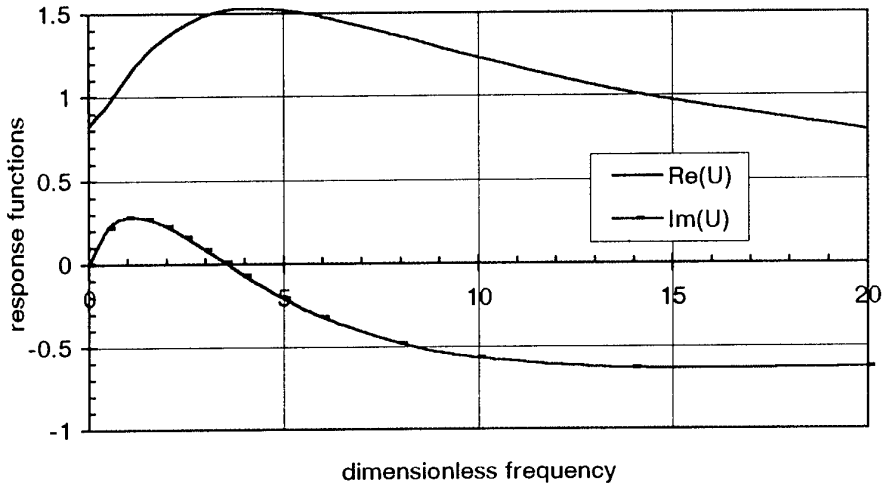

Figure 19: Response functions of mixture 1
at 10 atm, To=20°C

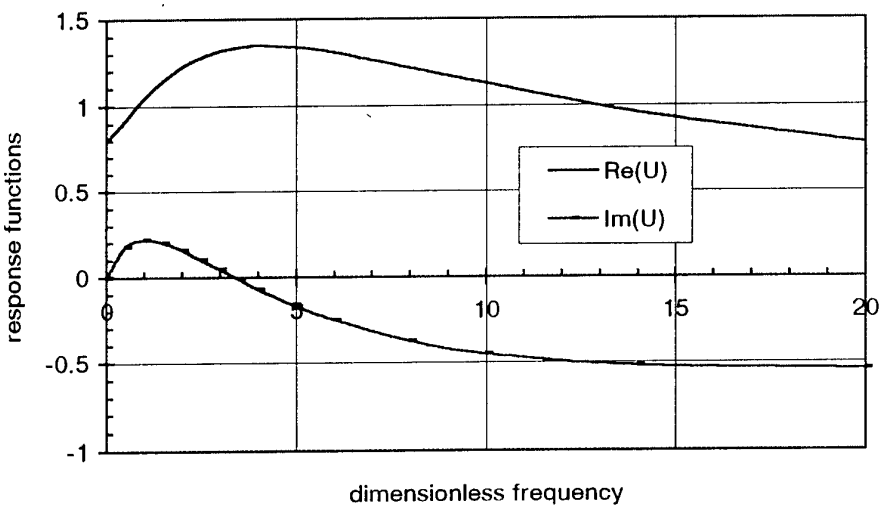

Figure 20: Response functions of mixture 1
at 20 atm, To=20°C

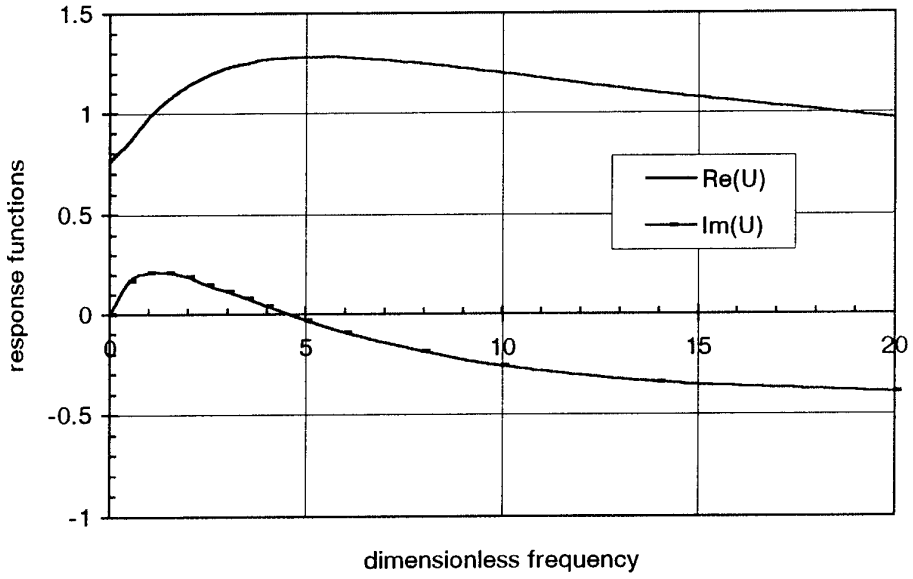

Figure 21: Response functions of mixture 1
at 50 atm, To=20'C

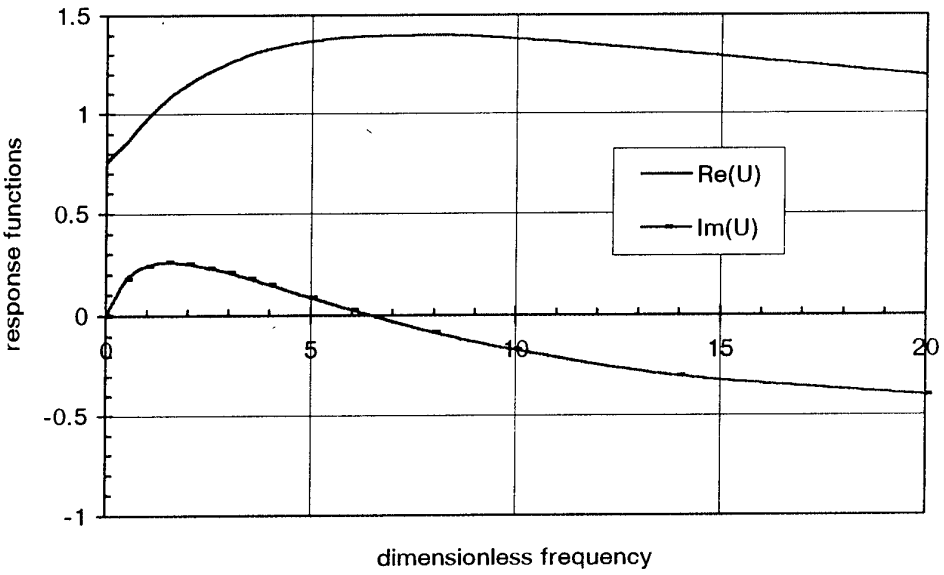

Figure 22: Response functions of mixture 1
at 100 atm, To=20'C